Hydrol. Earth Syst. Sci., 27, 1667–1682, 2023
https://doi.org/10.5194/hess-27-1667-2023

Hydrology and Earth System Sciences
Open Access
EGU

Elucidating the role of soil hydraulic properties on aspect-dependent landslide initiation

Yanglin Guo[1,2] **and Chao Ma**[1,2]

[1]School of Soil and Water Conservation, Beijing Forestry University, Beijing 100083, PR China
[2]Jixian National Forest Ecosystem Observation and Research Station,
CNERN, Beijing Forestry University, Beijing 100083, PR China

Correspondence: Chao Ma (sanguoxumei@163.com)

Received: 16 August 2022 – Discussion started: 31 August 2022
Revised: 15 March 2023 – Accepted: 29 March 2023 – Published: 20 April 2023

Abstract. Aspect-dependent landslide initiation is an interesting finding, and previous studies have attributed this to the mechanical effects of plant roots. In the present study, an overwhelming landslide probability on a south-facing slope over a north-facing slope was found in a localized area with only granite underneath and high cover of *Larix kaempferi*. These observations cannot be attributed to plant roots but may result from factors related to hillslope hydrology. Differential weathering associated with hillslope hydrology behaviors such as rainfall water storage and leakage, pore water pressure, particle component, and hillslope stability fluctuation were used to examine these observations. Remote sensing interpretation using the high-resolution GeoEye-1 image, digitalized topography, and field investigations showed that landslides on south-facing slopes have a higher probability, larger basal area, and shallower depth than those on a north-facing slope. The lower limits of the upslope-contributing area and slope gradient condition for south-facing landslides were less than those for north-facing landslides. The higher basal areas of south-facing landslides than those of the north-facing landslides may be attributed to the high peak values and slow dissipation of pore water pressure. The absorbed and drained water flow in a given time interval, together with the calculated water storage and leakage measured during the rainy season, demonstrate that the soil mass above the failure zone for south-facing slope is more prone to pore water pressure, which results in slope failures. In comparison, the two stability fluctuation results from the finite and infinite models further verified that landslides on south-facing slopes may fail under conditions of prolonged antecedent precipitation and intensive rainfall. Meanwhile, those on north-facing slopes may fail only in response to intensive rainfall. The results of this study will deepen our knowledge of aspect-dependent landslide initiation from both classical mechanics and the state of stress.

1 Introduction

In some semi-arid environments of the Northern Hemisphere, aspect-dependent landslide initiation provides valuable insights into the relative importance of different factors in developing accurate landslide susceptibility models (Ebel et al., 2015; Rengers et al., 2016; Li et al., 2021; Deng et al., 2022). These events provide a thorough understanding of the amount of direct sunlight that translates into differences in vegetation communities, bedrock weathering, and soil development processes (Fu, 1983; Wang, 2008; Bierman and Montgomery, 2014). These Earth surface processes indirectly affect hillslope hydrology and landscape dissection at the hillslope scale. Rainfall-induced shallow landslides are geomorphic agents at the hillslope scale and are governed by multiple factors, including hydrology, hillslope materials, bedrock, and vegetation (Birkeland, 1984; Geroy et al., 2011; Lu and Godt, 2013). Currently, the aspect-dependent landslide initiation observed has been predominantly attributed to the mechanical effect of plant roots. This is because the differences in vegetation on the south- and north-facing slopes are easier to examine and more pronounced than other factors (Li et al., 2021; Timilsina et al., 2021; Dai et al., 2022; Deng et al., 2022). However, vegetation succession takes place over substantially shorter timescales than soil devel-

opment and bedrock weathering (Watakabe and Matsushi, 2019). In most cases, the plant roots are not deep enough to penetrate the bedrock (Schwinning, 2010). Hypothesizing for a relatively localized area with the same ecosystem or plant species, aspect-dependent landslide initiation cannot be attributed to plant roots but may result from differences in the properties of hillslope materials due to long-term differential weathering.

Aspect-dependent landslides in Front Range, Colorado, USA, and the Loess Plateau, China, have attracted interest because the vegetation has a considerable influence on landslide distribution. The strong propensity for shallow landslide initiation on south-facing hillslopes in the two regions is closely related to the present-day tree density, regardless of the hillslope aspect (Ebel et al., 2015; Rengers et al., 2016; Deng et al., 2022). In the Colorado Front Range, field observations have shown that south-facing slopes lack thick tree cover and have an abundance of rock outcrops compared to north-facing slopes. In addition, the soil layer is thinner on south-facing slopes (Coe et al., 2014; Ebel et al., 2015). The cohesion supplied by the roots is responsible for the connection observed between the landslide distribution and slope aspect (McGuire et al., 2016). On the Loess Plateau, China, vegetation recovery is one of the main ecological measures for mitigating sediment loss (Fu et al., 2009). Increased soil strength and hydraulic conductivity due to strong root networks may enhance the topographic initiation conditions (Montgomery and Dietrich, 1994; Wang et al., 2020). These studies highlight the effect of the mechanical function of plants on landslides. North- and westward moving storms may potentially produce more intense rainfall on the south- and east-facing slopes. This assumption may be invalid if an aspect-dependent landslide distribution is present in a localized catchment with a specific vegetation community. If an aspect-dependent landslide exists in a localized area with vegetation cover comprising the same plant species alongside a high level of vegetation cover, then the aspect-dependent landslide initiation observed cannot be attributed to the mechanical effect of plant roots.

To determine the relationship observed among vegetation, landslides, and slope aspect, the effects of the physical properties and strength of hillslope materials cannot be excluded. On the northern part of the Loess Plateau, China, and in many other semi-arid environments, different types and densities of vegetation and soils develop on north-facing versus south-facing convergent slopes (Fu, 1983; Heimsath et al., 1997; Wang, 2008). This is because systematic differences in the amount of direct sunlight translate into differences in physical and chemical weathering. North-facing convergent slopes have lower evaporation rates, retain snow cover longer in spring, and tend to hold soil moisture longer during the summer growing season. These differences may result in localized ecosystem communities in the presence of trees or shrubs on grass. South-facing slopes experience heavier and more frequent hydration, thermal expansion, or freeze–thaw cycles due to day warming and night cooling and tend to have stronger weathering throughout the year. These differences can result in local differences in the grain component, soil strength, and soil profile. This has indirect effects at the landslide scale through the mechanics of excessive pore water pressure dissipation and sliding surface liquefaction (Terzaghi, 1950; Sassa, 1984) and hillslope hydrology behavior (Godt et al., 2009; Lee and Kim, 2019). Therefore, the physical properties of hillslope materials may be attributed to the aspect-dependent landslide initiation observed.

Shallow landslides are examples of debris flow initiation, which often enlarges their scale by multiple mechanics (Hungr et al., 2005; Iverson et al., 2011). When the slope fails, the pore water pressure abruptly increases within the shear zone (Iverson and LaHusen, 1989; Wang and Sassa, 2003). If the excessive pore water pressure persists and is high over the static pressure for a relatively long duration, then the displaced masses may enlarge their volume by widespread liquefaction and transform into debris flows (Bogaard and Greco, 2016). The magnitude of the pore water pressure is closely related to the scale of shallow landslide. Therefore, the scale of shallow landslides can be determined by excessive pore water pressure during the failure process. However, the aspect-dependent landslide distribution in these two areas refers to the differences in landslide probability rather than the landslide scale.

In the present study, we used a combination of field soil moisture observation, strength measurement, hydraulic conductivity analysis of hillslope materials, and numerical modeling of slope stability to explain the high potential for landslide initiation on south-facing slopes relative to north-facing slopes with the same vegetation communities. Differences in landslide geometry and initiation conditions, in the form of the contributing area above the scar area and the landslide gradient, were shown using field investigations and high-resolution GeoEye-1 images. The differential weathering-related physical properties and strength of the soil mass, including the dry unit weights, porosity, grain size, effective cohesion, and inner friction angle, were examined. We have also highlighted the importance of excessive pore water pressure, hillslope hydrology, and stability in explaining the aspect-dependent landslide initiation observed. The results of this work will deepen our understanding of aspect-dependent landslide distribution in some mountainous areas of the Northern Hemisphere.

2 Study area

The study area is in the mountainous region of Majiaba village, northeast of Niangniangba town, Tianshui city, Gansu province, central China. It is also close to the dividing crest of the Yellow and Yangtze rivers and on the eastern part of the Loess Plateau. The elevation of the mountain near Niangniangba town in the mountain region of the study area

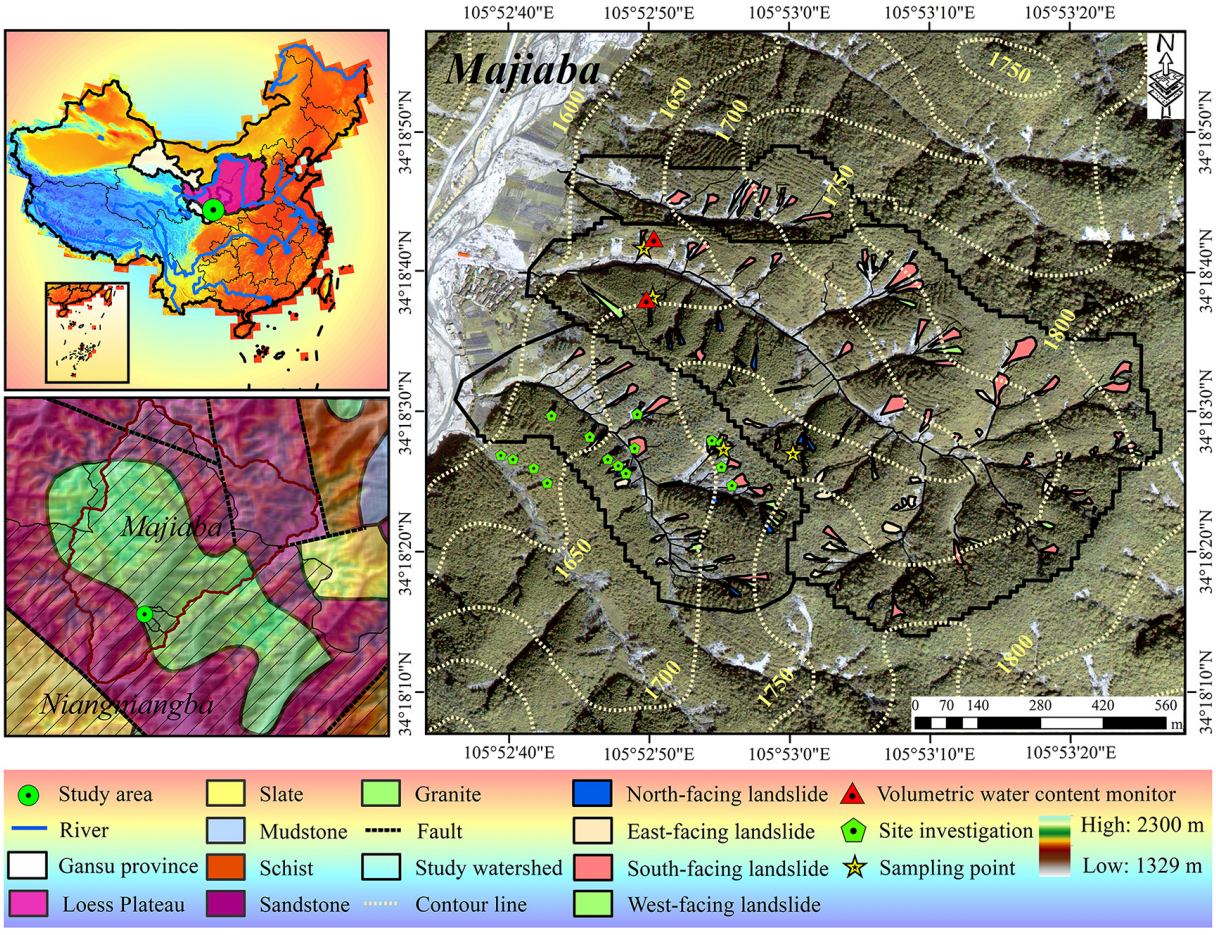

Figure 1. Location, topography, and simplified lithology of the study area. All maps are created by the authors. The graph of Majiaba was taken using an unmanned aerial vehicle. The territorial domain of China and the simplified lithology map are from the China Geological Survey. The elevation legend refers to the mountain area spanning Niangniangba and Majiaba.

ranges from 1329 to 2300 m. Most of the hillslope is underlain by sandstone, and the stratigraphic units of granite, slate, schist, and mudstone account for a smaller area. This area has four distinctive seasons and a semi-humid climate. The annual precipitation is approximately 491.6 mm and predominantly falls during June and August. One branch fault of the Tianshui–Lanzhou fault system runs through the area and has had no rupture records for the last few decades.

The shallow landslides in the study area and nearby surroundings were triggered by the prolonged antecedent precipitation during 1–24 July and the intensive rainstorm on 25 July 2013 (Yu et al., 2014; Guo et al., 2015). Most shallow landslides during the entire storm spanned the mountain area with a gradient of 20–25°, located on south-facing slopes, and in areas with relatively low vegetation coverage (Li et al., 2021). Besides, some works found that plant roots may increase the topographical initiation threshold of landslides because of their positive effect on the strength and hydraulic conductivity of soil–root composite (Dai et al., 2022). The three small catchment areas in the Majiaba watershed are underlain by granite units. The total area is 0.88 km^2, with vegetation cover of over 90 % (Fig. 1). The relative relief was approximately 200 m, and the mean hillslope gradient was 37°. The reason why the three catchments in the area were chosen is that the main plant species on the south- and north-facing slope is *Larix kaempferi*, which commonly has highly developed lateral roots with depth < 0.4 m. However, landslides in the three catchments still have a higher occurrence propensity on south-facing slopes in comparison with the north-facing slopes. This finding differs from the results from Front Range, Colorado, USA, and the Central Loess Plateau, China, where landslides commonly occur in sparsely vegetated areas. Li et al. (2021) only addressed the relationship between landslide probability and vegetation cover at the regional scale, while excluding the importance of the properties of hillslope materials at a more localized scale. Therefore, we hypothesize that such observations in the study area may not be the result of the mechanical effect of plant roots but may be from the distinctive physical properties and the strength of hillslope materials due to differential weathering.

3 Materials and methods

3.1 Landslide information interpretation

The high-resolution GeoEye-1 image (0.5 m × 0.5 m) on 8 October 2013 was orthorectified, and the landslide boundary was visually interpreted using ENVI 5.1 and e-Cognition 8 software. An unmanned aerial vehicle (UAV) was used to obtain a digital elevation model (DEM) with a 5 m resolution. The GeoEye-1 orthographic image and DEM were spatially registered in ArcGIS 10.2 as a standard layer of an orthoimage. The landslide initiation condition is represented by the competition between the slope gradient and upslope contribution area ($A - S$) as follows:

$$S = kA^{-b}, \tag{1}$$

where S is the local slope ($\mathrm{m\,m^{-1}}$), A is the contribution area above the landslide head scar ($\mathrm{m^2}$), k is an empirical constant related to lithology, vegetation, and climate, and b is an empirically defined index.

Field studies were conducted to measure the depth of the head scar and sidewall area using tape, and the failure depth was taken as their average. The landslide volume could then be calculated using the interpreted scar area and failure depth measured. Detailed landside information including the landslide number and area probability, landslide volume and width, head scar and sidewall depth, and the upslope-contributing area–slope gradient condition for the south- and north-facing slopes were compared.

3.2 Field monitoring and soil sampling

To investigate the hillslope hydrology on south- and north-facing slopes, frequency domain reflectometry (FDR) soil moisture sensors were used in this work to record the volumetric water content. To avoid the randomness of the data caused by natural factors such as terrain and vegetation, a total of 16 shallow landslides were investigated to excavate soil profiles and take undisturbed soil samples. Sensors were installed at depths of 30, 70, and 110 cm on the south- and north-facing slopes to monitor the volumetric water content during June and September 2021. Soil moisture monitoring was implemented at two concave sites on the south- and north-facing slopes. The meteorological station was less than 3 km away from the study area to record the rainfall on a 30 min basis. During the sensor installation, undisturbed soil samples near the sensor location were taken for indoor tests, including the dry unit weight, porosity, grain size, shear strength, and hydraulic conductivity. The grain size was analyzed using a Malvern Mastersizer 3000 instrument (Malvern, UK). In each layer, at least four samples were collected for the consolidated undrained triaxial compression test (CU). Two samples were collected for unsaturated hydraulic conductivity measurement using transient release and imbibition tests (Lu and Godt, 2013). Saturated hydraulic conductivity was determined using the constant water head method (Table 1).

3.3 Pore water pressure dissipation

CU tests were performed to obtain the effective cohesion, effective internal friction angle, and pore water pressure curves. Soil samples with a diameter of 50 mm and height of 100 mm were first saturated in a vacuum pump. They were then consolidated in the chamber of GDS apparatus (GDS Instruments, UK) at 50, 100, 150, and 200 kPa confining pressures and 10 kPa back pressure. During each test, the shear rate was set to $0.1\,\mathrm{mm\,min^{-1}}$, and the device automatically recorded data every 10 s. Owing to the varied particle components and soil texture, the increasing and dissipation ratios of pore water pressure differentiate a lot. As a highly excessive pore water pressure and slow dissipation ratio could cause widespread Coulomb failure within the shear zone, it will influence the landslide scale. To compare the rate of the rise and dissipation of pore water pressure during the CU test, the ratio is expressed as follows:

$$i = \frac{p_{t+\Delta t} - p_t}{\Delta t}, \tag{2}$$

where i is the increase or dissipation ratio of the excessive pore water pressure, and p_t and $p_{t+\Delta t}$ are the pore water pressures measured during the time interval of Δt. A higher i indicates that the pore water within the soil mass drains rapidly, and the pore water pressure will dissipate in a short time. In other words, the i is a proxy representing the hydraulic conductivity.

3.4 Water storage and drainage

The unsaturated permeability of soil mass (diameter 61.8 mm; height 25.4 mm) was measured using the transient release and imbibition method (TRIM; Lu and Godt, 2013). In this test, the water outflow mass was measured on a 10 min basis. In each test, air pressures of 250 and 0 kPa corresponded to the drying and wetting processes, respectively. The soil water characteristic curve (SWCC) and hydraulic conductivity function (HCF) were obtained using Hydrus 1D (Wayllace and Lu, 2012). Using the models proposed by Mualem (1976) and Van Genuchten (1980), the constitutive relations between the suction head (h), water content (θ), and hydraulic conductivity (K) under drying and wetting states can be represented by the following equation:

$$\frac{\theta - \theta_\mathrm{r}}{\theta_\mathrm{s} - \theta_\mathrm{r}} = \left[\frac{1}{1 + (\alpha\,|h|)^n}\right]^{1-\frac{1}{n}}, \tag{3}$$

and

$$K = K_\mathrm{s}\frac{\left\{1 - (\alpha\,|h|)^{n-1}\left[1 + (\alpha\,|h|)^n\right]^{\frac{1}{n}-1}\right\}^2}{\left[1 + (\alpha\,|h|)^n\right]^{\frac{1}{2}-\frac{1}{2n}}}, \tag{4}$$

Table 1. Physical properties and strength parameters of the soil mass.

Parameters	South-facing slope			North-facing slope		
	Layer 1	Layer 2	Layer 3	Layer 1	Layer 2	Layer 3
Unit weight of soil ($kN\,m^{-3}$)	14.8	15.6	17.2	14	16.6	17.1
Porosity (%)	43.0	43.1	36.2	42.5	37.3	36.4
Effective cohesion (kPa)	6.5	17.5	21.2	5.3	9.1	7.9
Effective inner friction angle (°)	29.8	25	31	27.1	35.2	41
Saturated hydraulic conductivity ($cm\,s^{-1}$)	6.4×10^{-3}	6.2×10^{-4}	4.4×10^{-4}	8.8×10^{-3}	1.2×10^{-3}	4.3×10^{-3}

where θ_r is the residual moisture content (%), θ_s is the saturated moisture content (%), α and n are empirical fitting parameters, α is the inverse of the air entry pressure head, n is the pore size distribution parameter, and K_s is the saturated hydraulic conductivity ($cm\,s^{-1}$).

The soil water storage (S_s) and drainage (S_d) during a rainfall event can be evaluated by the soil depth and the difference between the maximum soil moisture and antecedent soil moisture, as follows:

$$S_e = \frac{\theta - \theta_r}{\theta_s - \theta_r} \tag{5}$$

$$S_s = S_e^w \Delta h \tag{6}$$

$$S_d = P - S_e^d \Delta h, \tag{7}$$

where S_e is the degree of saturation, θ is the volumetric moisture content measured (%), Δh is the average soil thickness (400 mm in this study), S_e^w and S_e^d are the residual soil moisture in the wetting and drying processes (%), and P is the accumulated rainfall (mm).

3.5 Stability fluctuation

In this study, we applied a finite and infinite stability model to assess the slope stability fluctuation during the rainy season as an attempt to examine aspect-dependent landslide initiation from the perspective of classical mechanics and the state of stress (Schmidt et al., 2001). The finite-slope model evaluates the stability F_s', as follows:

$$F_s' = \frac{c_l A_l + c_b A_b + A_b\left(\rho_s - \rho_\omega S_e\right) g z \cos^2\beta \tan\varphi'}{A_b \rho_s g z \sin\beta\cos\beta}, \tag{8}$$

where β is the topographic slope angle (°), A_l is the lateral area of side wall (m^2), A_b is the basal area (m^2), z is the sliding depth (m), c_l is the effective cohesion along the sidewall (kPa) and adopts the cohesion of layer 1 and layer 2, c_b is the basal soil cohesion (kPa) and adopts the cohesion of layer 3, ρ_s is the soil particle density ($g\,cm^{-3}$), and ρ_w is the water density ($g\,cm^{-3}$).

The infinite slope stability model in this study provides insight into the stress variation resulting from changes in the soil suction and water content during infiltration (Lu and Likos, 2006):

$$F_s'' = \frac{\tan\varphi'}{\tan\beta} + \frac{2c'}{\gamma z \sin 2\beta} - \frac{\sigma^s}{\gamma z}(\tan\beta + \cot\beta)\tan\varphi', \tag{9}$$

where φ' is the effective friction angle (°), β is the topographic slope angle (°), c' is the effective cohesion (kPa), and γ is the unit weight of the soil ($kN\,m^{-3}$). σ^s is the suction stress (kPa), which is expressed as follows:

$$\sigma^s = -\frac{S_e}{\alpha}\left(S_e^{n/(1-n)} - 1\right)^{1/n}. \tag{10}$$

4 Results

4.1 Shallow landslides on south- and north-facing slope

In the study area, direct sunlight does not coincide with the aspect orientation because it is to the north of the Tropic of Cancer. The south-facing slope is defined between 157.5 and 247.5°, and the north-facing slope is between 0 to 67.5° and 292.5 to 360° (0° is due north). There were 71 shallow landslides on the south-facing slope and 20 landslides on the north-facing slope in the study area. Figure 2a shows that shallow landslides on south-facing slopes have larger spatial areas than those on north-facing slopes. Most of the shallow landslides occurred on the south-facing slope (Fig. 2b). The volume of landslides on the south-facing slope was greater than that on the north-facing slope. For landslides on the south-facing slope, the basal area was 372.64 m^2, and the width was 14.9 m on average. For landslides on the north-facing slope, the average basal area was 157.28 m^2, and the width was 7.7 m (Fig. 2c). Although the landslides on the south-facing slope had a larger volume and greater width, the depth of the head scar and sidewall area are no greater than those on the north-facing slope. Field studies showed that the averaged depth for landslides on the north-facing slope was 1.02 m, which was deeper than the depth of 0.83 m for landslides on south-facing slope (Fig. 2d). The landslides on the south-facing slope exhibited an overwhelming propensity for occurrence in terms of the number and area. Meanwhile, the failure depth was no more than that of the landslides on the north-facing slope.

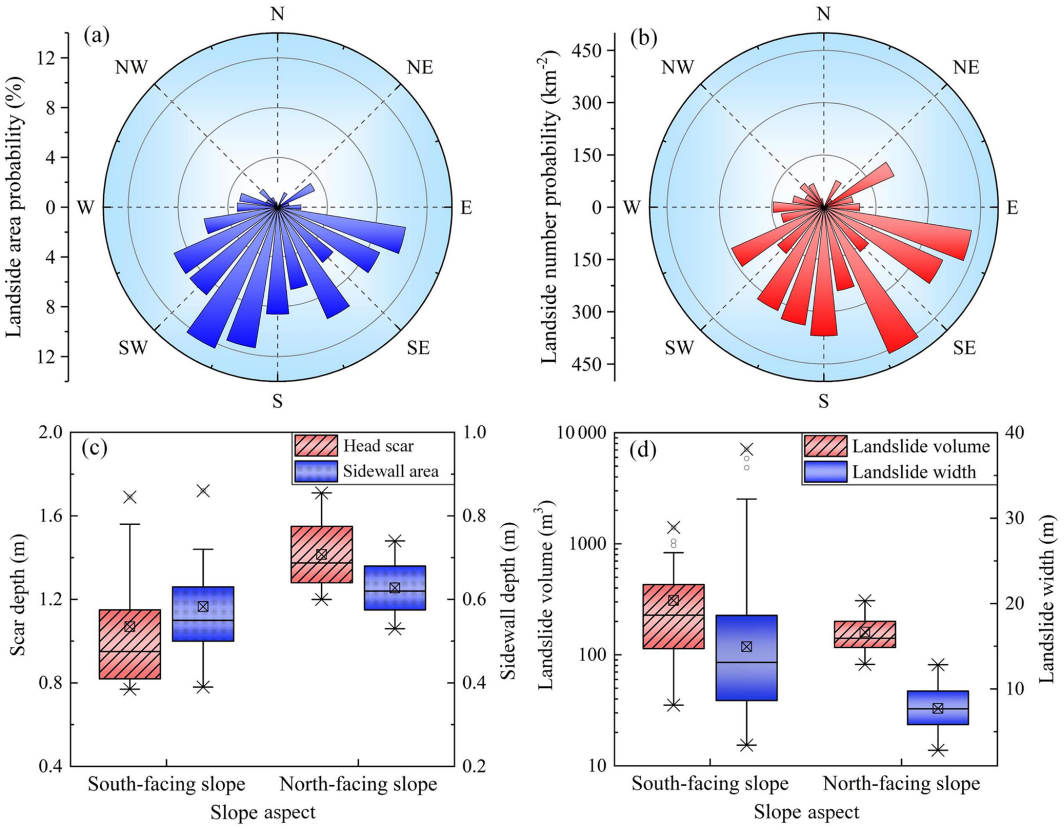

Figure 2. Spatial distribution and geometric characteristics of the landslide, including **(a)** landslide area probability vs. slope aspect, **(b)** landslide number probability vs. slope aspect, **(c)** landslide volume and width vs. slope aspect, and **(d)** scar depth and sidewall depth vs. slope aspect. The three crossing lines of box show the 75th quantile (Q_3), median (Q_2), and 25th quantile (Q_1) from top to bottom. The length of the box is referred to as the interquartile range (IQR $= Q_3 - Q_1$). The crossed square inside the box is the average value. The whiskers extend to the maximum and minimum values, except for the mild outliers. The upper limit and lower limit of whiskers are $Q_3 + 1.5$IQR and $Q_1 - 1.5$IQR, respectively. The circles are the outliers, and the cross symbol is the maximum and minimum values for all the data.

Shallow landslides can be modeled as occurring when sufficient through-flow converges from the upslope contribution area to the hollow area and triggers slope instability (Montgomery and Dietrich, 1994). Their topographic initiation conditions are controlled by the spatial competition between the slope and the upslope contribution being area dependent (Stock and Dietrich, 2003, 2006; Horton et al., 2008). For the shallow landslides in the study area, the averaged upslope-contributing area and slope gradient did not significantly differ (Fig. 3a). Meanwhile, the lower limit line representing the minimum initiation condition for landslides on south-facing slopes was lower than that on the north-facing slopes (Fig. 3b). This indicates that a higher upslope contribution area was required to provide sufficient through-flow conditions and trigger slope failures on the north-facing slope. Given that the landslides in the study area were triggered by prolonged antecedent precipitation and intensive rainfall (Li et al., 2021), sufficient rainfall infiltration could result in a high soil water content within the displaced mass, leading to a decrease in matric suction and soil strength. The generation of pore water pressure in response to intense rainfall also plays an important role in shallow landslides. Therefore, we have proposed two assumptions to elucidate the distribution and scale of aspect-dependent landslides. The first assumption is that the basal area of the landslide may be related to the soil strength and high pore water pressure. This assumption can be tested by the pore water properties, including the pore water generation potential and dissipation ratio during the failure process. The second assumption is that the south-facing slope may have a higher failure potential than the north-facing slope in a given rainfall process. This can be determined from the stability comparison using Eqs. (8) and (9).

4.2 Differences in soil physical properties

To show the differences in the physical properties of the hillslope materials, the dry unit weights, porosity, and grain size distribution of the soil mass in the three layers on each slope were compared (Fig. 4). The effective cohesion and inner

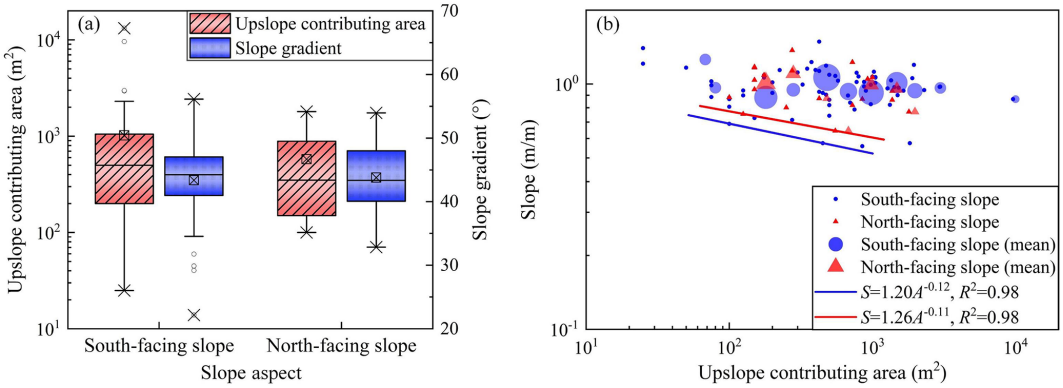

Figure 3. Upslope-contributing area and slope gradient condition, with the **(a)** upslope-contributing area and mean slope vs. slope aspect and **(b)** the upslope-contributing area vs. mean slope gradient above the landslide area. The definitions of the whiskers are shown in the caption of Fig. 2. The circles are averaged slopes, with the radius size proportional to the number of landslides. The small circles and triangles represent all individual data values. The power law regression is fitted with the dataset closet to the axis origin.

friction angle were then examined with respect to the particle component (Table 1 and Fig. 5).

For the soil mass on the south-facing slope, the dry unit weights increased with soil depth, whereas the porosity and saturated hydraulic conductivity decreased (Fig. 4a and Table 1). For soil layers 1 and 2, the soil textures were similar because the proportions of sand, silt, and clay did not differ significantly. However, the proportion of silt in soil layer no. 3 was no more than that in layer nos. 1 and 2, and the sand proportion was higher. The average failure depth was above soil layer no. 3 and below soil layer no. 2. For the soil mass on the north-facing slope, the dry unit weight also increased with soil depth. Unlike the south-facing slope, the porosity of the soil mass for the three soil layers was approximately 38 % and did not differ among them. For the soil texture, the proportion of sand in soil layer no. 1 was no more than that in soil layer nos. 2 and 3 (Fig. 4b). The depth of the failure plane was close to that of soil layer 3.

In comparison, one of the main difference was the higher saturated hydraulic conductivity for the soil mass above the failure plane on the north-facing slope. This may have resulted from the high porosity and sand proportion. This indicates that the rainfall infiltration on the north-facing slope could penetrate faster than that of the south-facing slope. The soil mass of the three layers on the south-facing slope had a higher proportion of fine particles than those on the north-facing slope if gravel was considered (Fig. 5). The saturated hydraulic conductivity for the soil masses from soil layer nos. 2 and 3 on the south-facing slope was lower than that on the north-facing slope. This is expected because the porosity and proportion of fines on the south-facing slope were higher.

According to the results of the triaxial shear test (Table 1), the soil mass in each layer on the north-facing slope had a smaller effective cohesion than that on the south-facing slope. The effective cohesion on the failure plane for landslides on the south-facing slope may be twice that on the north-facing slope. However, the effective inner friction angles for the soil masses of soil layers 2 and 3 on the north-facing slope were far greater than those on the south-facing slope. These differences in effective cohesion and inner frictional angle may be attributed to the higher clay and silt and fewer coarse grains within the soil mass on the south-facing slope.

4.3 Pore water pressure properties

The consolidation module of the triaxial shear test was used to measure the generation and dissipation process of the pore water pressure. The principle is to consolidate and drain soil from the initial saturated state. Under the same confining pressure, there are pronounced differences in the consolidation rate, consolidation time, and peak rise in pore water pressure for different soil properties. The results of the pore water pressure during the consolidation process under 200 kPa effective confining pressure were compared here (Fig. 6). The peak value of pore water pressure within the soil mass on the south-facing slope was higher than that on the north-facing slope. The peak value of the pore water pressure within the soil mass on the south-facing slope increased to 150–200 kPa. However, the peak value of pore water pressure within the soil mass on the north-facing slope was below 150 kPa. Both the rising and decaying rates of pore water pressure for soil mass layers 1 and 2 on the south-facing slope were lower than those on the north-facing slope. The rate and decaying rates for soil mass layer no. 2 on the south-facing slope were 1.2 and −0.031 kPa per 10 s, respectively. However, they were 9.6 and −0.765 kPa per 10 s for the soil mass on the north-facing slope.

The lower peak pore water pressure demonstrates the effect of fine particles on the pore water pressure, which directly affects landslide mobility and scale. Rainfall-induced landslides result from an increase in positive pore water pres-

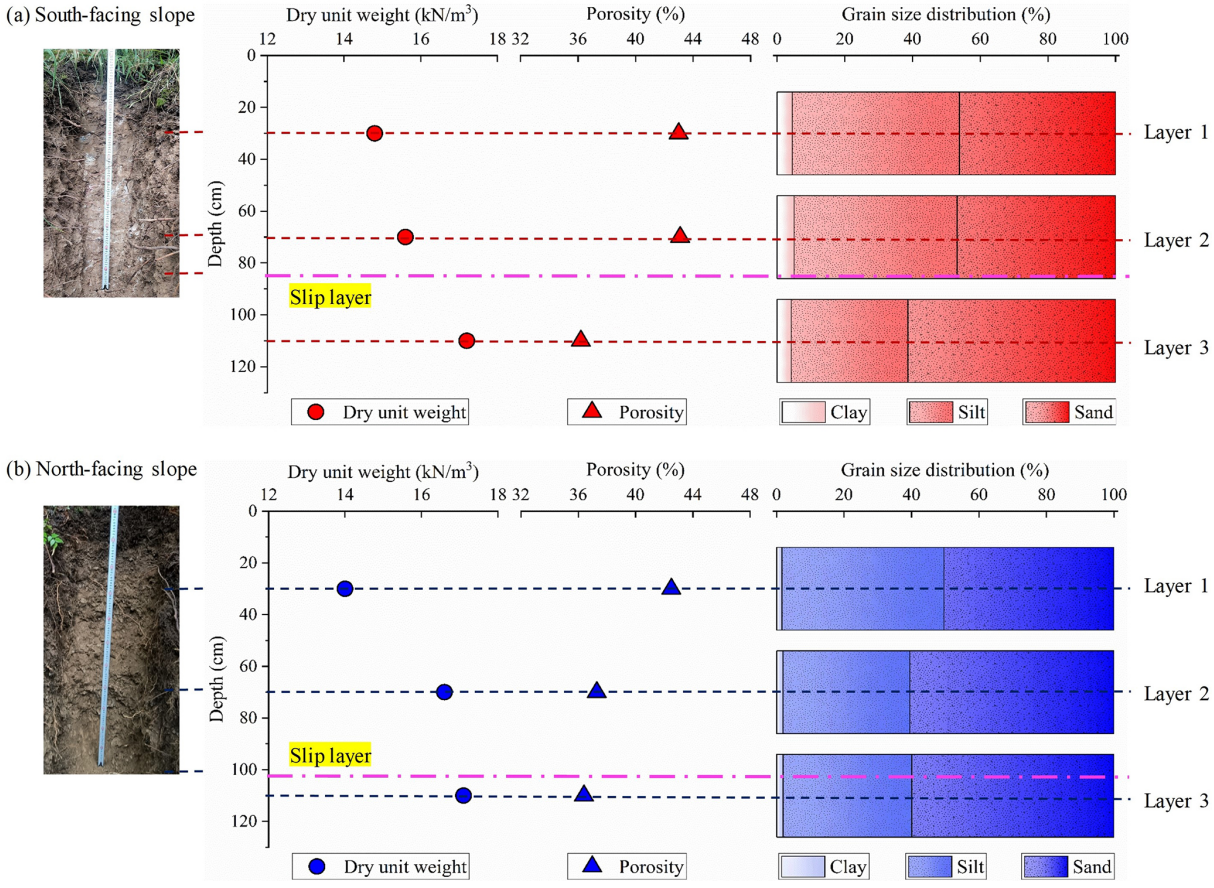

Figure 4. Differences in the soil properties including dry unit weights, porosity, and grain size in sand, silt, and clay. **(a)** Physical properties of soil mass on the south-facing slope and **(b)** physical properties of soil mass on the north-facing slope. The two soil profile photos were taken by Yanglin Guo during the field investigation.

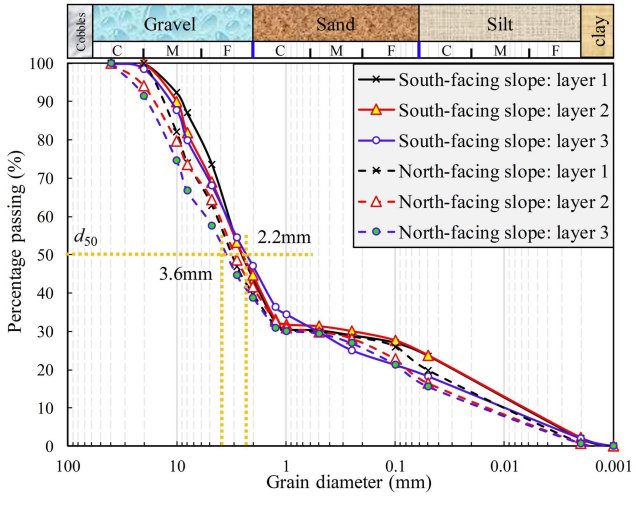

Figure 5. Soil particle component curves. The letters C, M, and F mark the coarse, medium, and fine scale.

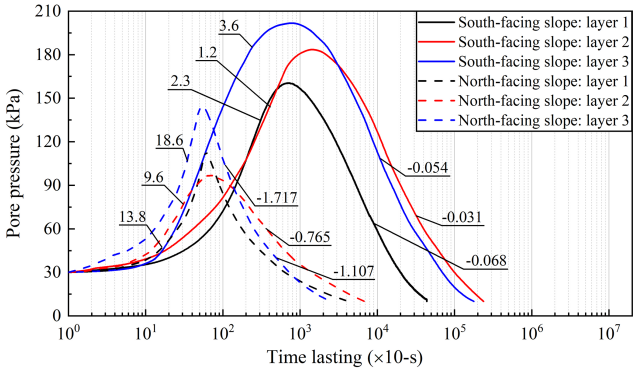

Figure 6. Variation in pore water pressure under an effective confining pressure of 200 kPa by GDS triaxial shear tests (GDS Instruments, UK). The values in Fig. 6 are the average rates of the rise and dissipation of pore water pressure during consolidation calculated by Eq. (2). The unit of the x axis marks the time record interval of 10 s.

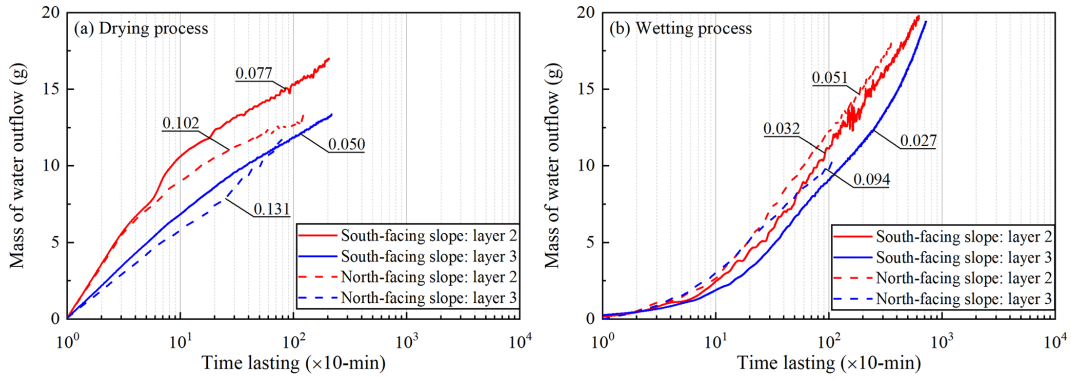

Figure 7. Mass of water outflow during the drying and wetting process, including **(a)** drying tests and **(b)** wetting tests. The mass of water outflow was recorded at 10 min for each test.

sure within the failure plane, which reduces the effective stress and shear strength of the soil (Terzaghi, 1950). This often occurs in the undrained soil layer, which can easily cause slope liquefaction (Sassa, 1984). The increase in pore water pressure predominantly depends on the speed of landslide movement, soil deformation, and soil permeability. If the shear rate is given, then the dissipation rate of pore water pressure for high-permeability soil is faster, and therefore, the increase in pore pressure is smaller (Iverson and LaHusen, 1989; Iverson et al., 1997). As shown in Table 1, the saturated hydraulic conductivity for the soil mass of layer nos. 2 and 3 on the north-facing slope was 10 times that of the south-facing slope. Therefore, the peak pore water pressure measured during the test for the soil mass on the south-facing slope was higher. The soil mass on the north-facing slope had higher sand and gravel contents than that on the south-facing slope (Fig. 5). A high clay content on the south-facing slope filled the macropores within the soil mass and reduced the pore water discharge rate. Wang and Sassa (2003) found that fine particles play the most important role in the dissipation of pore pressure. The pore water pressure within the saturated sand increased with shear rate. The soil mass with high coarse particles produced less pore water pressure than the soil with high fine particles during the shear process. Therefore, the high permeability of the soil mass on the north-facing slope may result in low peak pore water pressure. The higher fine particles may result in a slow increase and dissipation of the pore water pressure. This slow pore water pressure dissipation could result in the liquefaction failure of the sliding mass and a larger landslide area.

4.4 Unsaturated hydraulic conductivity

4.4.1 Measured water outflow mass

Figure 7 shows the water outflow mass measured for a given 10 min period during the drying and wetting processes. The water outflow masses measured for soil layers 2 and 3 on the north-facing slope were generally higher than those on the south-facing slope. For the drying tests using the soil mass of soil layer nos. 2 and 3 on the north-facing slope, the given water outflow masses were 0.10 and 0.131 g per 10 min, respectively. However, the water outflow masses measured for the soil mass of soil layer nos. 2 and 3 were 0.077 and 0.050 g per 10 min, respectively, on the south-facing slope (Fig. 7a). For tests using the same layers of the soil mass in the wetting process, the water outflow masses measured were 0.051 and 0.094 g per 10 min on the north-facing slope, respectively, and 0.032 and 0.027 g per 10 min, respectively, on the south-facing slope (Fig. 7b). Overall, the permeability of the soil mass on the north-facing slope was higher than that on the south-facing slope. The same results were obtained when the saturated hydraulic conductivities of the soil layers were measured using the constant water head method (Table 1).

4.4.2 SWCC and HCF curves

The soil water characteristic curve (SWCC) and hydraulic conductivity function (HCF) are critical for the analysis of water flow movement and the mechanical behavior of unsaturated soil material. In this study, the transient release and imbibition method (TRIM) for unsaturated hydraulic property measurement is used (Lu and Godt, 2013). The advantage of the TRIM method is that it combines physical experiments and calibration. It employs a relatively simple and reliable measurement of transient water content using an electronic balance to record the signature of transient unsaturated flow. It also takes advantage of the robust inverse modeling capability to simulate the physical process. The apparatus could accommodate both undisturbed and remolded samples. The results of this study were obtained using the Hydrus-1D code with the reverse modeling option, and the Levenberg–Marquardt nonlinear optimization algorithm. This minimized the error between the results of the test and the simulation (Wayllace and Lu, 2012). Meanwhile, to ensure the uniqueness of the parameters, the algorithm repeatedly runs with different initial parameter estimates until it converges to obtain the same or similar results. The pre-

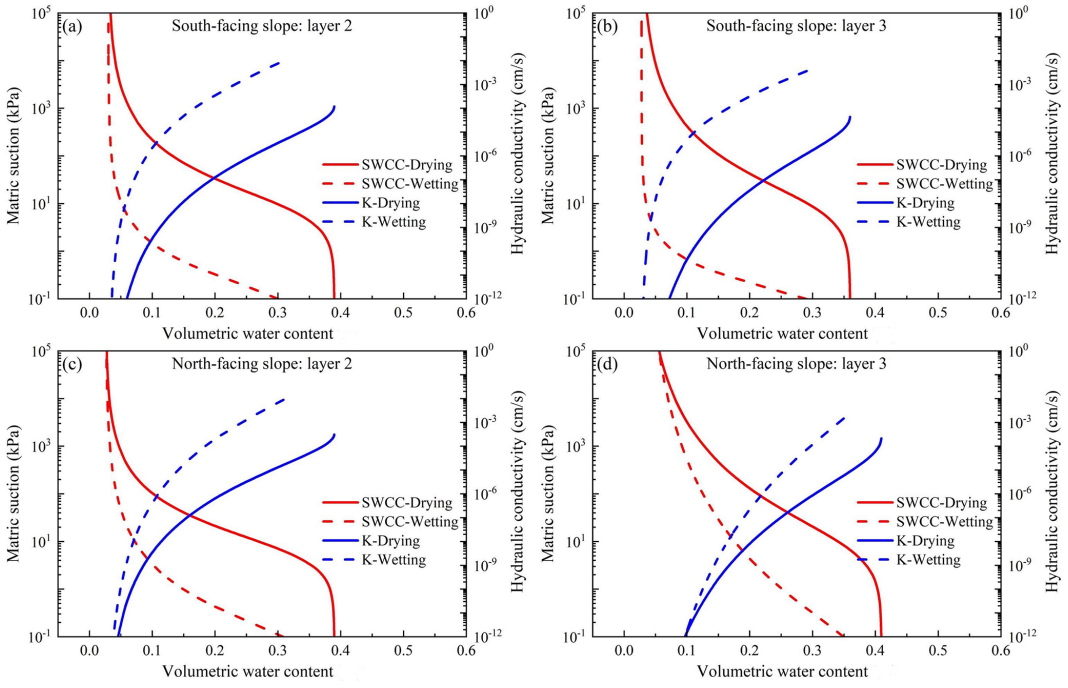

Figure 8. Soil water curve obtained using the TRIM test, where **(a)** layer no. 2 is on the south-facing slope, **(b)** layer no. 3 is on the south-facing slope, **(c)** layer no. 2 is on the north-facing slope, and **(d)** layer no. 3 is on the north-facing slope.

diction results are then compared with the function curves of water flow and time obtained from the actual experiment so that they can be combined to meet certain accuracy requirements. In this experiment, the R^2 of the regression between the optimized predicted value and the observed value was greater than 0.99. The model constraint effect of the TRIM under two suction increment steps was better, and the parameters obtained by the inversion calculation were more accurate (Lu and Godt, 2013). Table 2 shows the soil parameters obtained using the Hydrus 1D inversion.

Using these parameters, the SWCC and HCF curves of the soil mass at soil layers 2 and 3 on the north- and south-facing slopes can be drawn (Fig. 8). Air entry pressure and residual water content are two important parameters that describe the hydrological and mechanical characteristics of the hillslope materials. The air entry pressure represents the critical value at which air enters the saturated soil and starts to drain. For soil layer no. 2, the difference between the air entry values of the north- and south-facing slopes can reach 14.03 kPa (Fig. 8a and c). The residual water content and air entry pressure of the south-facing slope were higher than those of the north-facing slope. For soil layer no. 3, the soil mass on the north-facing slope has the smallest air entry pressure, which is 0.51 times that of the air entry pressure of the south-facing slope (Fig. 8b and d). The saturated hydraulic conductivities of soil layer nos. 2 and 3 on the south-facing slope were lower than those on the north-facing slope in both the drying and wetting processes. The saturated hydraulic conductivity of the soil mass on the north-facing slope in the wetting test was 1 order of magnitude higher than that on the south-facing slope. In Table 1, the saturated permeability coefficient measured by the constant head test method also shows that the soil mass on the north-facing slope has higher permeability. These results suggest that it is more difficult for the soil mass on south-facing slope to absorb and drain water than the soil mass on the north-facing slope.

4.5 Water storage and drainage

To show the water storage during the rainfall process and the water drainage after the rainfall, the timely recorded soil moisture at various soil layers and the rainfall process during 11 June and 20 August were used (Fig. 9a and b). In comparison, this is likely the most important finding, as it shows that the soil becomes nearly saturated on the south slope but not on the north slope. This implies that the soil water on the south-facing slope has difficulty in draining water because of the presence of more fine grains and slow pore water pressure dissipation. The stable soil moisture from soil layer nos. 2 and 3 for both slopes may be attributed to the long dry seasons in the study area. The daily rainfall amount > 30 mm on 9 and 23 July resulted in an increase in soil moisture for all the slope layers.

Figure 10a shows that the storied water of the north- and south-facing slopes did not synchronously increase with accumulated precipitation. When the storied water rapidly increased, then the increase in soil water storage of the north-facing slope was greater than that of the south-facing slope.

Table 2. Parameters describing the soil and water characteristic curve (SWCC) and the hydraulic conductivity function (HCF) from Hydrus 1D.

Parameters	Definition	South-facing slope		North-facing slope	
		Layer 2	Layer 3	Layer 2	Layer 3
θ_r	Residual moisture	0.0302	0.0278	0.0262	0.0268
θ_s^d	Saturated moisture	0.39	0.36	0.39	0.41
θ_s^w		0.36	0.38	0.39	0.42
α^d (kPa^{-1})	The inverse of the air entry pressure head	0.0128	0.0117	0.0156	0.0141
α^w (kPa^{-1})		0.78	0.94	1.21	1.86
n^d	The pore size distribution parameter	1.49	1.39	1.57	1.27
n^w		1.63	1.85	1.43	1.18
K_s^d (cm s^{-1})	Saturated hydraulic conductivity	1.52×10^{-4}	0.64×10^{-4}	3.76×10^{-4}	4.56×10^{-4}
K_s^w (cm s^{-1})		9.58×10^{-2}	4.93×10^{-2}	4.10×10^{-1}	4.68×10^{-1}

Note that the superscripts "d" and "w" indicate drying and wetting states.

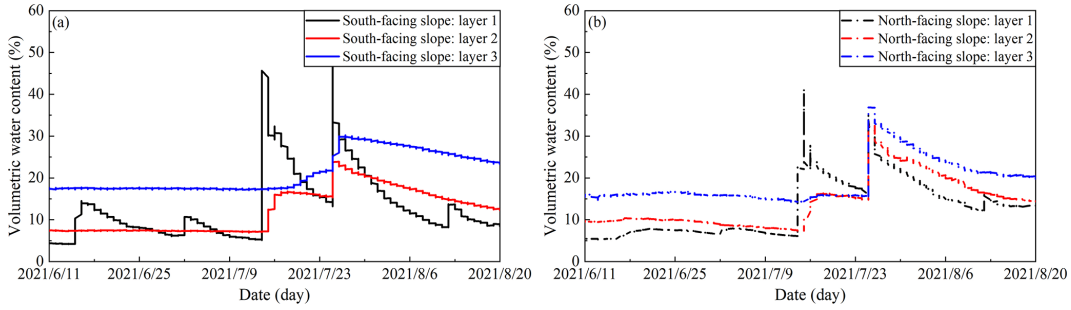

Figure 9. Field-monitored volumetric water content, including **(a)** soil moisture on the south-facing slope and **(b)** soil moisture on the north-facing slope.

On 26 July, a rainfall of 30.8 mm h^{-1} was recorded, and the water storage of the slope reached the peak. The peak of the water storage on the north-facing slope was higher than that of the south-facing slope. However, when the accumulated rainfall tends to be stable; that is, when the rainfall stops for a period, then the decline rate of the soil water storage on the north-facing slope is substantially higher than that on the south-facing slope. The soil water storage of the south-facing slope was always higher than that of the north-facing slope during rainfall. During the drainage process, the seepage rate of the north-facing slope was greater than that of the south-facing slope (Fig. 10b). Therefore, the south-facing slope had a better water storage performance, and the north-facing slope had a higher drainage performance.

4.6 Stability fluctuation

In this study, the infinite slope model and the finite slope model were used to characterize the sensitivity of landslide triggering to determine the main mechanism of high landslide probability on south-facing slopes. The infinite slope model can be used to examine the transient stress changes caused by water entering the soil, emphasizing the differences in soil permeability (Lu and Likos, 2006; Lu and Godt, 2013). The finite slope model focuses on the cohesion of the base surface and lateral periphery of the ground landslide source body, in addition to the influence of the additional lateral cohesion provided by the vegetation root system for the landslide (Schmidt et al., 2001; Dai et al., 2022).

Figure 11a shows the rainfall records from 11 June to 20 August 2021. In general, the degree of saturation of the sliding layer on the south-facing slope was higher than that on the north-facing slope (Fig. 11b). In the finite model, the stability of the south-facing slope was always higher than that of the north-facing slope (Fig. 11c). In the infinite model, the stability of the north-facing slope was generally higher than that of the south-facing slope, and the stability of the north-facing slope fluctuated substantially (Fig. 11d). On 26 July, a rainfall event with a maximum intensity of 30.8 mm h^{-1} resulted in a sudden decrease in stability. The estimated stability index of the north-facing slope decreased to become lower than that of the south-facing slope and then increased afterwards. Although the soil moisture of the south-facing slope

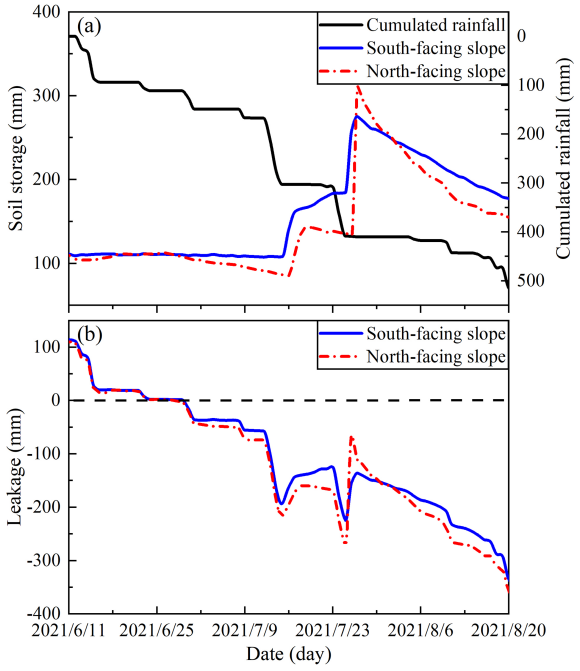

Figure 10. Seepage model of slope water storage and drainage. **(a)** Soil water storage. **(b)** Soil water drainage.

increased substantially during the rainfall event on 16 July, the stability fluctuation was relatively small. This may be related to the relatively strong effective cohesion and smaller pore structure. In the finite slope model, the results have shown that the south-facing slope has a relatively high stability. However, this result contradicts the high landslide density on the south-facing slope in the study area. In fact, the finite slope model does not consider suction stress, and the effective cohesion of hillslope materials mainly affects the stability result. In contrast, the results of the infinite slope model asserts that the state of the stress of the soil or regolith is modified by infiltration and changes in soil matrix suction. Furthermore, the fluctuation in Fig. 11d also proves that the role of infiltration of water into shallow soils and the subsequent pore water pressure response at depth is critical to the understanding the transient conditions that lead to shallow slope failure because the stability fluctuation amplitude of the south-facing hillslope was smaller than that of the north-facing hillslope. This indicated that the water movement on the south-facing slope was less active than that of the north-facing slope. Therefore, in the study area, the change in soil suction stress was more sensitive to slope stability than the change in root–soil cohesion. The change in soil permeability caused by differential weathering of the bedrock could be responsible for aspect-dependent landslide initiation in the study area.

5 Discussion

The strong propensity for landslides in some arid environments in the Northern Hemisphere is scientifically interesting, and some researchers have highlighted the contribution of plant roots. This finding is to be expected in the future in other mountain regions, where water is a limiting factor for local system sustainability. In the Colorado Front Range, McGuire et al. (2016) found that the apparent cohesion supplied by roots was responsible for the connection observed between the landslide distribution and slope aspect (Ebel et al., 2015; Rengers et al., 2016). In the study area, Li et al. (2021) also found that plant roots may explain the connection observed between vegetation cover and landslide probability for the entire study area. Dai et al. (2022) found that a strong root network and high saturated hydraulic conductivity may promote the $A - S$ condition of shallow landslides. On the Loess Plateau in China, some researchers have observed that the strong propensity for shallow landslide initiation is closely related to the present-day tree density, and plant roots do not penetrate over the failure plane (Guo et al., 2020; Deng et al., 2022). However, the strong propensity for shallow landslides on north- and south-facing slopes cannot be attributed to plant roots because the artificial vegetation on both slopes is the same. Conversely, these observations could be the result of the soil hydraulic and mechanical properties from differential weathering.

This study has contributed to knowledge of the effect of differential weathering on aspect-dependent landslide initiation from the perspective of soil hydraulic properties, in addition to the mechanical and hydrological effects of plant roots. Except for the strong propensity for a high number of landslides, shallow landslides on the south-facing slopes have exhibited larger areas and greater widths than those on the north-facing slopes (Fig. 2). This may be attributed to the slow dissipation of excessive pore water pressure because widespread liquefaction may extend the landslide scale. For the thinner slip layer of landslides on south-facing slope, it may result from differential weathering because the theoretical maximum or maximum slip layer for a strong cohesive slope should be larger than a weak cohesive slope at given slope (Iida, 1999; D'Odorico and Fagherazzi, 2003). One of the reasons may be that cohesive soil masses often hold together tightly to displace downslope, owing to the strength loss. The relatively weak cohesive soil mass often loosens to displace downslope, with the slip layer close to the boundary between soil mass and bedrock underneath. However, a stronger effective cohesion tends to promote the $A - S$ conditions of shallow landslides. A larger upslope-contributing area or steeper gradient is required to trigger slope failure. Figure 3 shows that some shallow landslides on south-facing slopes fail at lower upslope-contributing areas. Therefore, soil-hydraulic-property-related factors, such as the rising or dissipation of pore water pressure, water storage, and drainage, may contribute to the phenomena observed.

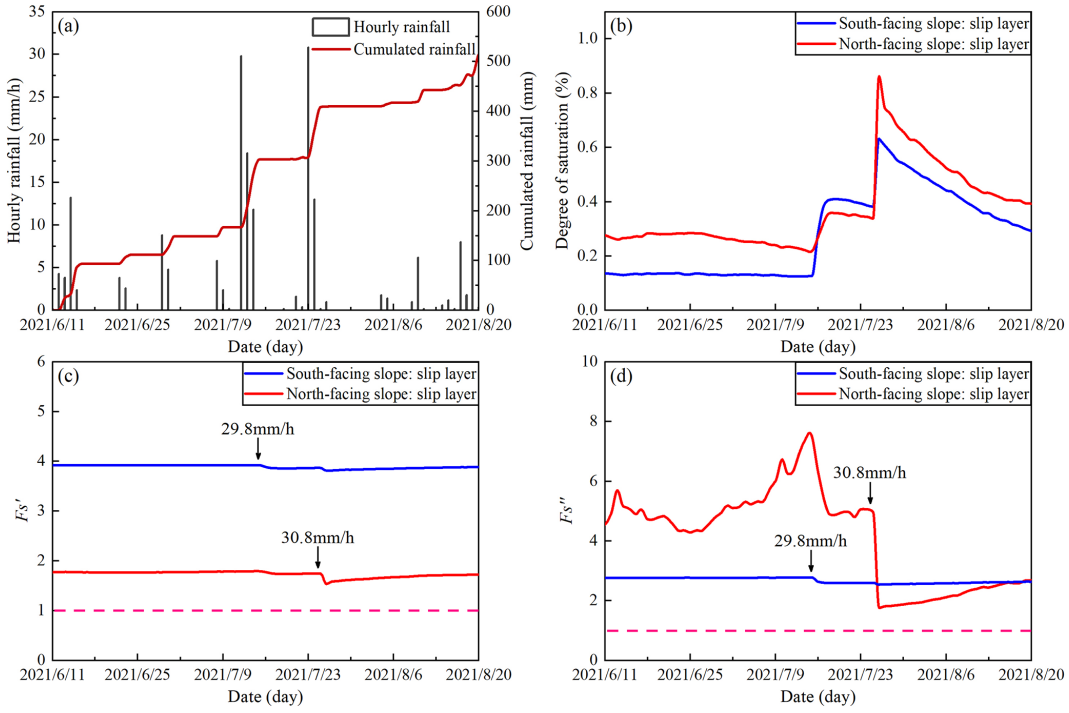

Figure 11. Change in slope stability fluctuation shown by the **(a)** rainfall records, **(b)** degree of saturation, **(c)** stability of finite slope model, and **(d)** stability of infinite slope model. The dotted pink lines indicate the stability index of 1.0.

The saturated hydraulic conductivities obtained by the constant water head and TRIM methods coincide, which demonstrates that the hillslope material on the north-facing slope has a larger water infiltration (Tables 1 and 2). However, the difference between K_s^d and K_s^w is strikingly high, and the K_s^d is smaller. Although the TRIM test in this work measures the permeability of the soil matrix, the influence of other factors, such as the soil development and weathering, preferential flow pathway, and macro pore, cannot be ignored (Lohse and Dietrich, 2005; Maier et al., 2020), and the contribution of such an influence on the permeability rate cannot be evaluated at present. The stability results, using the finite and infinite models, imply that the failure potential of landslides on a north-facing slope is lower than that on a south-facing slope because the stability index of a south-facing slope is always close to 1.0. These differences imply that slope failures on a north-facing slope may only occur under intensive rainfall conditions or by a combination of prolonged antecedent precipitation and short-duration, intensive rainfall. For potential failures on the south-facing slopes, the combination of prolonged antecedent precipitation and short-duration, intensive rainfall should be a potential trigger, owing to the low hydraulic conductivity and pore water pressure dissipation. This study highlights the role of hydraulic properties in landslide occurrence. Although the south- and north-facing slopes are underlain by granite, the physical properties of hillslope materials such as excessive pore water pressure, strength of sliding mass, soil water storage, and leakage are significantly different. One of the possible limitations of this work lies in the representativeness of the moisture observation and the uncertainty. Considering the multiple factors influencing landslides, the study area is selected with same bedrock underneath and similar plant species. Then, the moisture observation sites were selected on the condition that there were similar soil profiles, a landscape with the majority of landslides, and common topographical conditions. Therefore, this finding cannot be random because the study area has been selected on the condition that it is relatively far from the northern and eastern region, where local soils are predominantly loess deposits, and the study areas of Li et al. (2021) and Dai et al. (2022), where the bedrock underneath differs substantially. The main purpose of this work is to elucidate the reason for aspect-dependent landslide initiation from the perspective of soil hydraulic properties. These differences result from differential weathering owing to the amount of direct sunlight. Other methods such as numerical or relative dating methods and preferential flow in the macropore distribution could provide new evidence for such observations.

6 Conclusion

Previous research on the strong propensity for shallow landslides on south-facing slopes over north-facing slopes has highlighted the role of plant roots. In a localized area with

the same vegetation including plant roots, they do not penetrate the failure layer. Such an overwhelming landslide phenomenon cannot be attributed to plant roots and may result from the differential weathering of bedrock under the influence of hydrothermal conditions. In this study, we jointly explained the soil hydraulic properties from physical and mechanical properties, pore water pressure, unsaturated hydraulic conductivity, water storage and drainage, and slope stability fluctuation during monitoring and studied landslide initiation related to slope direction. The following conclusions were drawn.

1. In terms of soil physical and mechanical properties on both slopes, the soil masses on the south-facing slope have a higher silt content than those on the north-facing slope. The effective cohesion of the soil mass on the south-facing slope was higher than that on the north-facing slope, while the effective frictional angle was smaller.

2. The results of the GDS tests (GDS Instruments, UK) showed that the dissipation rate of pore water pressure for soil mass on the south-facing slope was substantially lower than that on the north-facing slope. Higher effective cohesion and slower pore water pressure dissipation may result in a larger basal area for shallow landslides on south-facing slopes.

3. The soil mass on the south-facing slope had a higher residual water content and air entry pressure and a lower saturated hydraulic conductivity than that of the north-facing slope. For water storage and drainage performance, the storied water from the south-facing slope was higher than that of the north-facing slope, while the north-facing slope had a higher leakage rate. The results of the stability analysis based on the finite and infinite models show that the infinite slope model may be suitable for elucidating aspect-dependent landslide distribution in the study area.

Code and data availability. The raw/processed data in this work can be made available upon request to the corresponding author.

Author contributions. CM found the strong propensity for shallow landslide initiation on south-facing hillslopes in the study area and launched a research proposal. YG completed the sampling collection and indoor tests.

Competing interests. The contact author has declared that neither of the authors has any competing interests.

Disclaimer. Publisher's note: Copernicus Publications remains neutral with regard to jurisdictional claims in published maps and institutional affiliations.

Special issue statement. This article is part of the special issue "Experiments in Hydrology and Hydraulics". It is not associated with a conference.

Acknowledgements. The authors sincerely thank the contributions of other colleges, including Muyang Li, Zhisheng Dai, Lv Miao, Lijuan Wang, and Jiayong Deng, for their previous work near the study area.

Financial support. This research has been supported by the State Key Program of Natural Science of China (grant no. 42130701), the Natural Science Foundation of China (grant no. 42177309), and the Fundamental Research Funds for the Central Universities (grant no. 2018BLCB03).

Review statement. This paper was edited by Jorge Isidoro and reviewed by Tammo Steenhuis, Jan Wienhöfer, and two anonymous referees.

References

Bierman, P. R. and Montgomery, D. R.: Key Concepts in Geomorphology, W. H. Freeman and Company Publishers, ISBN 13:9781429238601, 2014.

Birkeland, P. W.: Soils and Geomorphology, New York: Oxford University Press, ISBN 13:9780195033984, 1984.

Bogaard, T. A. and Greco, R.: Landslide hydrology: from hydrology to pore pressure, Wiley Interdisciplin. Rev. Water, 3, 439–459, https://doi.org/10.1002/wat2.1126, 2016.

Coe, J. A., Kean, J. W., Godt, J. W., Baum, R. L., Jones, E. S., Gochis, D. J., and Anderson, G. S.: New insights into debris-flow hazards from an extraordinary event in the Colorado front range, GSA Today, 24, 4–10, https://doi.org/10.1130/GSATG214A.1, 2014.

Dai, Z. S., Ma, C., Miao, L., Li, M. Y., Wu, J. L., and Wang, X. H.: Initiation conditions of shallow landslides in two man-made forests and back estimation of the possible rainfall threshold, Landslides, 19, 1031–1044, https://doi.org/10.1007/s10346-021-01823-1, 2022.

Deng, J. Y., Ma, C., and Zhang, Y.: Shallow landslide characteristics and its response to vegetation by example of July 2013, extreme rainstorm, Central Loess Plateau, China, Bull. Eng. Geol. Environ., 81, 100, https://doi.org/10.1007/s10064-022-02606-1, 2022.

D'Odorico, P. and Fagherazzi, S.: A probabilistic model of rainfall-triggered shallow landslides in hollows: A long-term analysis, Water Resour. Res., 39, 1262, https://doi.org/10.1029/2002WR001595, 2003.

Ebel, B. A., Rengers, F. K., and Tucker, G. E.: Aspect-dependent soil saturation and insight into debris-flow initiation during extreme rainfall in the Colorado front range, Geology, 43, 659–662, https://doi.org/10.1130/G36741.1, 2015.

Fu, B. J., Wang, Y. F., Lu, Y. H., He, C. S., Chen, L. D., and Song, C. J.: The effects of land-use combinations on soil erosion: a case study in the Loess Plateau of China, Prog. Phys. Geogr., 33, 793–804, https://doi.org/10.1177/0309133309350264, 2009.

Fu, B. P.: Mountain climate, Science Press, ISBN 130312413, 1983.

Godt, J. W., Baum, R. L., and Lu, N.: Landsliding in partially saturated materials, Geophys. Res. Lett., 36, L02403, https://doi.org/10.1029/2008GL035996, 2009.

Geroy, I. J., Gribb, M. M., Marshall, H. P., Chandler, D. G., Benner, S. G., and McNamara, J. P.: Aspect influences on soil water retention and storage, Hydrol. Process., 25, 3836–3842, https://doi.org/10.1002/hyp.8281, 2011.

Guo, F. Y., Meng, X. Y., Li, Z. H., Xie, Z. T., Chen, G., and He, Y. F.: Characteristics and causes of assembled geo-hazards induced by the rainstorm on 25th July 2013 in Tianshui City, Gansu, China, Mt. Res., 33, 100–107, 2015.

Guo, W. Z., Chen, Z. X., Wang, W. L., Gao, W. W., Guo, M. M., Kang, H. L., Li, P. F., Wang, W. X., and Zhao, M.: Telling a different story: The promote role of vegetation in the initiation of shallow landslides during rainfall on the Chinese Loess Plateau, Geomorphology, 350, 106879, https://doi.org/10.1016/j.geomorph.2019.106879, 2020.

Heimsath, A. M., Deitrich, W. E., Nishizumi, K., and Frinkel, R. C.: The soil production function and landscape equilibrium, Nature, 388, 358–361, https://doi.org/10.1038/41056, 1997.

Horton, P., Jaboyedoff, M., and Bardou, E.: Debris flow susceptibility mapping at a regional scale, in: Proceedings of the 4th Canadian Conference on Geohazards, edited by: Locat, J., Perret, D., Turmel, D., Demers, D., and Leroueil, S., 20–24 May 2008, Québec, Canada, 399–406, https://www.researchgate.net/publication/259174917 (last access: 18 April 2023), 2008.

Hungr, O., McDougall, S., and Bovis, M.: Entrainment of material by debris flows, in: Debris-flow Hazards and Related Phenomena, Springer Praxis Books, Springer, Berlin, Heidelberg, https://doi.org/10.1007/3-540-27129-5_7, 2005.

Iida, T.: A stochastic hydro-geomorphological model for shallow landsliding due to rainstorm, Catena, 34, 293–313, https://doi.org/10.1016/S0341-8162(98)00093-9, 1999.

Iverson, R. M. and LaHusen, R. G.: Dynamic pore-pressure fluctuations in rapidly shearing granular materials, Science, 246, 796–799, https://doi.org/10.1126/science.246.4931.796, 1989.

Iverson, R. M., Reid, M. E., and LaHusen, R. G.: Debris-flow mobilization from landslides, Annu. Rev. Earth Planet. Sci., 25, 85–138, https://doi.org/10.1146/annurev.earth.25.1.85, 1997.

Iverson, R. M., Reid, M. E., Logan, M., Lahusen, R. G., Godt, J. W., and Griswold, J. P.: Positive feedback and momentum growth during debris-flow entrainment of wet bed sediment, Nat. Geosci., 4, 116–121, https://doi.org/10.1038/ngeo1040, 2011.

Lee, E. and Kim, S.: Seasonal and spatial characterization of soil moisture and soil water tension in a steep hillslope, J. Hydrol., 568, 676–685, https://doi.org/10.1016/j.jhydrol.2018.11.027, 2019.

Li, M. Y., Ma, C., Du, C., Yang, W. T., Lyu, L. Q., and Wang, X. H.: Landslide response to vegetation by example of July 25–26, 2013, extreme rainstorm, Tianshui, Gansu Province, China, Bull. Eng. Geol. Environ., 80, 751–764, https://doi.org/10.1007/s10064-020-02000-9, 2021.

Lohse, K. A. and Dietrich, W. E.: Contrasting effects of soil development on hydrological properties and flow paths, Water Resour. Res., 41, 1–17, https://doi.org/10.1029/2004WR003403, 2005.

Lu, N. and Godt, J. W.: Hillslope hydrology and stability, Cambridge Univ. Press, Cambridge, UK, ISBN 13:9781107021068, 2013.

Lu, N. and Likos, W. J.: Suction stress characteristic of unsaturated soils, J. Geotech. Geoenviron. Eng., 132, 131–142, https://doi.org/10.1061/(ASCE)1090-0241(2006)132:2(131), 2006.

Maier, F., van Meerveld, I., Greinwald, K., Gebauer, T., Lustenberger, F., Hartmann, A., and Musso, A.: Effects of soil and vegetation development on surface hydrological properties of moraines in the Swiss Alps, Catena, 187, 104353, https://doi.org/10.1016/j.catena.2019.104353, 2020.

McGuire, L. A., Rengers, F. K., Kean, J. W., Coe, J. A., Mirus, B. B., Baum, R. L., and Godt, J. W.: Elucidating the role of vegetation in the initiation of rainfall-induced shallow landslides: insights from an extreme rainfall event in the Colorado front range, Geophys. Res. Lett., 43, 9084–9092, https://doi.org/10.1002/2016GL070741, 2016.

Montgomery, D. R. and Dietrich, W. E.: Landscape dissection and drainage area-slope thresholds, in: Process models and theoretical geomorphology, edited by: Kirkby, M. J., John Wiley, Hoboken, NJ, 221–246, ISBN 10:0471941042, 1994.

Mualem, Y.: Hysteretical models for prediction of the hydraulic conductivity of unsaturated porous media, Water Resour. Res., 12, 1248–1254, https://doi.org/10.1029/WR012i006p01248, 1976.

Rengers, F. K., McGuire, L. A., Coe, J. A., Kean, J. W., Baum, R. L., Staley, D. M., and Godt, J. W.: The influence of vegetation on debris-flow initiation during extreme rainfall in the northern Colorado front range, Geology, 44, 823–826, https://doi.org/10.1130/G38096.1, 2016.

Sassa, K.: The mechanism starting liquefied landslides and debris flows, in: vol. 2, Proceedings of 4th International Symposium on Landslides, Toronto, Canada, 349–354, https://cir.nii.ac.jp/crid/1570009749923838464 (last access: 19 April 2023), 1984.

Schmidt, K. M., Roering, J. J., Stock, J. D., Dietrich, W. E., Montgomery, D. R., and Schaub, T.: The variability of root cohesion as an influence on shallow landslide susceptibility in the Oregon Coast Range, Can. Geotech., 38, 995–1024, https://doi.org/10.1139/t01-031, 2001.

Schwinning, S.: The ecohydrology of roots in rocks, Ecohydrology: Ecosystems, land and water process interactions, Ecohydrology, 3, 238–245, https://doi.org/10.1002/eco.134, 2010.

Stock, J. and Dietrich, W. E.: Valley incision by debris flows: evidence of a topographic signature, Water Resour. Res., 39, 1089, https://doi.org/10.1029/2001WR001057, 2003.

Stock, J. and Dietrich, W. E.: Erosion of steepland valleys by debris flows, Geol. Soc. Am. Bull., 118, 1125–1148, https://doi.org/10.1130/B25902.1, 2006.

Terzaghi, K.: Mechanism of landslides, in: Application of Geology to Engineering Practice (Berkey Volume), edited by: Paige, S., Geological Society of America, New York, 83–123, ISBN 13:9780813759418, 1950.

Timilsina, S., Niemann, J. D., Rathburn, S. L., Rengers, F. K., and Nelson, P. A.: Modeling hydrologic processes associated with soil saturation and debris flow initiation during the September 2013 storm, Colorado Front Range, Landslides, 18, 1741–1759, https://doi.org/10.1007/s10346-020-01582-5, 2021.

Van Genuchten, M. T.: A closed-form equation for predicting the hydraulic conductivity of unsaturated soils, Soil Sci. Soc. Am. J., 44, 892–898, https://doi.org/10.2136/sssaj1980.03615995004400050002x, 1980.

Wang, C. Y.: Study on the relationship between aspect and slope stability, Dissertation, Kunming University of Science and Technology, https://cdmd.cnki.com.cn/Article/CDMD-10674-2008112383.htm (last access: 18 April 2023), 2008.

Wang, G. H. and Sassa, K.: Pore-pressure generation and movement of rainfall-induced landslides: effects of grain size and fine-particle content, Eng. Geol., 69, 109–125, https://doi.org/10.1016/S0013-7952(02)00268-5, 2003.

Wang, X. H., Ma, C., Wang, Y. Q., Wang, Y. J., Li, T., Dai, Z. S., and Li, M. Y.: Effect of root architecture on rainfall threshold for slope stability: variabilities in saturated hydraulic conductivity and strength of root-soil composite, Landslides, 17, 1965–1977, https://doi.org/10.1007/s10346-020-01422-6, 2020.

Watakabe, T. and Matsushi, Y.: Lithological controls on hydrological processes that trigger shallow landslides: Observations from granite and hornfels hillslopes in Hiroshima, Japan, Catena, 180, 55–68, https://doi.org/10.1016/j.catena.2019.04.010, 2019.

Wayllace, A. and Lu, N.: A transient water release and imbibitions method for rapidly measuring wetting and drying soil water retention and hydraulic conductivity functions, Geotech. Test. J., 35, 1–15, 2012.

Yu, G. Q., Zhang, M. S., and Hu, W.: Analysis on the development characteristics and hydrodynamic conditions for massive debris flow in Tianshui, Northwest Geol., 47, 185–191, 2014.